SIAM J. SCI. COMPUT.
Vol. 17, No. 2, pp. 328-346, March 1996

002

HIGH-ACCURACY FINITE-DIFFERENCE SCHEMES FOR LINEAR WAVE PROPAGATION*

DAVID W. ZINGG†, HARVARD LOMAX‡, AND HENRY JURGENS†

Abstract. Two high-accuracy finite-difference schemes for simulating long-range linear wave propagation are presented: a maximum-order scheme and an optimized scheme. The schemes combine a seven-point spatial operator and an explicit six-stage low-storage time-march method of Runge–Kutta type. The maximum-order scheme can accurately simulate the propagation of waves over distances greater than five hundred wavelengths with a grid resolution of less than twenty points per wavelength. The optimized scheme is found by minimizing the maximum phase and amplitude errors for waves which are resolved with at least ten points per wavelength, based on Fourier error analysis. It is intended for simulations in which waves travel under three hundred wavelengths. For such cases, good accuracy is obtained with roughly ten points per wavelength.

Key words. finite-difference schemes, wave propagation, phase error, high accuracy

AMS subject classifications. 65M05, 76-08, 78-08

1. Introduction.

In the past few years, interest has grown in time-domain numerical simulations of linear wave phenomena using finite-difference or related methods. Applications include electromagnetic [12, 13, 20], acoustic [3, 6, 14], and elastic waves [10, 11]. It is generally recognized that in order to avoid excessively fine meshes for many practical problems, high-order discretizations are required. Consequently, many high-order differencing methods have been developed for problems involving wave phenomena [1, 4, 5, 7, 10].

Furthermore, optimized or spectral-like finite-difference schemes have been proposed which can provide improvements in accuracy over high-order schemes with the same computational effort [8, 9]. In an optimized finite-difference scheme, the error behavior over a range of spatial wavenumbers is optimized according to some criterion, usually based on Fourier error analysis. This contrasts with conventional schemes, which generally maximize the order of accuracy, i.e., the order of the leading error term. Detailed studies of optimized schemes have been performed by Lele [9] and Holberg [8], who optimized the spatial operator only. Sguazzero, Kindelan, and Kamel [11] have developed optimized fully discrete schemes based on Holberg's spatial operators. Tam and Webb [15] present an optimized scheme which consists of a seven-point centered-difference operator in space combined with a four-step time-marching method of the Adams–Bashforth type.

In this paper, we present two fully discrete finite-difference schemes for linear wave propagation: a maximum-order scheme and an optimized scheme. The schemes are suitable for problems requiring high accuracy with relatively large distances of travel. Both schemes combine a seven-point spatial operator and an explicit six-stage time-march method of the Runge–Kutta type. The spatial operator is divided into an antisymmetric component, i.e., a centered difference operator, and a symmetric component or filter. The optimized scheme is developed by minimizing the maximum phase and amplitude errors obtained using Fourier error analysis for waves which are resolved with at least ten points per wavelength.

The maximum-order scheme and the optimized scheme are presented in the next two sections. The two schemes are then analyzed and compared. Next, their stability is discussed and numerical boundary schemes are presented. After presenting the results of some numerical experiments, we conclude with a discussion of some of the considerations involved in choosing a difference scheme for a given problem.

*Received by the editors March 4, 1994; accepted for publication (in revised form) October 24, 1994.

†Institute for Aerospace Studies, University of Toronto, 4925 Dufferin Street, Downsview, Ontario, Canada M3H 5T6 (dwz@oddjob.utias.utoronto.ca, jurgens@oddjob.utias.utoronto.ca).

‡NASA Ames Research Center, Moffett Field, CA 94035 (lomax@nas.nasa.gov).

2. Maximum-order scheme. We consider first the spatial difference operator, which is divided into an antisymmetric component, i.e., a centered difference operator, and a symmetric component, or filter, which provides dissipation of high wavenumber modes. The grid is uniform with $x_j = j\Delta x$. The function values at the grid nodes are $u_j = u(x_j)$. For the linear convection equation with a positive phase speed, the first derivative of u at node j is approximated as

$$(\delta_x u)_j = \frac{1}{\Delta x}[(d_3 - a_3)u_{j-3} + (d_2 - a_2)u_{j-2} + (d_1 - a_1)u_{j-1} + d_0 u_j + (d_1 + a_1)u_{j+1} + (d_2 + a_2)u_{j+2} + (d_3 + a_3)u_{j+3}], \tag{1}$$

where the a_i are the coefficients of the antisymmetric component and the d_i are the coefficients of the filter. The maximum order of accuracy possible for this operator is sixth-order. This is obtained with $a_1 = 3/4$, $a_2 = -3/20$, $a_3 = 1/60$, $d_0 = d_1 = d_2 = d_3 = 0$. With a nonzero value of d_0, fifth-order accuracy is obtained with $d_1 = -3d_0/4$, $d_2 = 3d_0/10$, $d_3 = -d_0/20$.

Since the time-marching method described below is unstable for pure imaginary eigenvalues, a nonzero value of d_0 is required. We have chosen $d_0 = 0.1$. Although this introduces some amplitude error, the amplitude error of the fully discrete scheme is generally less than the phase error, as will be shown later. Furthermore, the resulting operator produces dissipation for high wavenumber components of the solution which are not propagated accurately.

In order to apply this spatial operator to a hyperbolic system of equations in the form

$$\frac{\partial \mathbf{u}}{\partial t} + \frac{\partial(\mathbf{Au})}{\partial x} = 0, \tag{2}$$

the operator must be split into the antisymmetric part, δ_x^a (with the a_i coefficients), and the symmetric part, δ_x^s (with the d_i coefficients). The spatial derivative in equation (2) is approximated as

$$\frac{\partial(\mathbf{Au})}{\partial x} \approx \delta_x^a \mathbf{Au} + \delta_x^s |\mathbf{A}|\mathbf{u} \tag{3}$$

where

$$|\mathbf{A}| = \mathbf{X}|\Lambda|\mathbf{X}^{-1}$$

and $\mathbf{X}$ is the matrix of right eigenvectors and Λ the matrix of eigenvalues of $\mathbf{A}$.

The time-marching method is an explicit six-stage method of the following form:

$$\begin{aligned} u_{n+\alpha_1}^{(1)} &= u_n + h\alpha_1 f_n, \\ u_{n+\alpha_2}^{(2)} &= u_n + h\alpha_2 f_{n+\alpha_1}^{(1)}, \\ u_{n+\alpha_3}^{(3)} &= u_n + h\alpha_3 f_{n+\alpha_2}^{(2)}, \\ u_{n+\alpha_4}^{(4)} &= u_n + h\alpha_4 f_{n+\alpha_3}^{(3)}, \\ u_{n+\alpha_5}^{(5)} &= u_n + h\alpha_5 f_{n+\alpha_4}^{(4)}, \\ u_{n+1} &= u_n + h f_{n+\alpha_5}^{(5)}, \end{aligned} \tag{4}$$

where $u_n = u(t_n)$, h is the time step, and

$$f^{(k)} = \frac{du^{(k)}}{dt}.$$

With $\alpha_5 = 1/2$, this method is second-order accurate. With $\alpha_5 = 1/2$, $\alpha_4 = 1/3$, $\alpha_3 = 1/4$, $\alpha_2 = 1/5$, $\alpha_1 = 1/6$, it produces sixth-order accuracy for linear homogeneous ordinary differential equations. In [19], this six-stage method is shown to be more accurate than the classical fourth-order Runge–Kutta method when combined with the above spatial operator for both homogeneous and inhomogeneous linear problems. The extra stages were accounted for by performing the comparison for an equal number of derivative function evaluations. Furthermore, the six-stage method requires less computer memory than the classical fourth-order Runge–Kutta method.

3. Optimized scheme. Optimized finite-difference schemes are obtained by dropping the requirement of maximum order of accuracy and selecting the resulting free parameters to achieve some desired error behavior. The spatial operator given in (1) is at least first-order accurate if

$$d_0 + 2d_1 + 2d_2 + 2d_3 = 0 \tag{5}$$

and

$$a_1 + 2a_2 + 3a_3 = \frac{1}{2}. \tag{6}$$

A value of $d_0 = 0.1$ was selected based on stability considerations and the need for high wavenumber damping, as discussed above. Therefore, by reducing the order of accuracy of the spatial operator to first order, four free parameters are obtained. The time-march method, (4), is at least second-order accurate as long as $\alpha_5 = 0.5$. With this constraint, four free parameters are available in the time-march method as well. Consequently, eight parameters are available to optimize the fully discrete scheme.

The present optimized scheme was developed to minimize the maximum error for waves resolved with at least ten grid points per wavelength (*PPW*) for Courant numbers less than or equal to one. There are numerous ways to find such an optimized scheme. We used the following approach. First, we determined the optimal spatial operator for the specified wavenumber range in one dimension. Using this spatial operator, we then optimized the time-march method at a Courant number of one, also in one dimension. The resulting coefficients are listed below:

$$\begin{gathered} a_1 = 0.7599613, \quad a_2 = -0.1581220, \quad a_3 = 0.01876090, \\ d_0 = 0.1, \quad d_1 = -0.07638461, \quad d_2 = 0.03228961, \quad d_3 = -0.005904994, \\ \alpha_1 = 0.168850, \quad \alpha_2 = 0.197348, \quad \alpha_3 = 0.250038, \quad \alpha_4 = 0.333306, \quad \alpha_5 = 0.5. \end{gathered} \tag{7}$$

4. Fourier error analysis. In order to analyze finite-difference schemes for wave propagation problems, we consider the linear convection equation [16], given in one dimension by

$$\frac{\partial U}{\partial t} + c\frac{\partial U}{\partial x} = 0, \tag{8}$$

where $U = U(x, t)$ and c, the phase speed, is a positive real constant. With an initial condition given by

$$U(x, 0) = U_0 \exp(i\kappa x), \tag{9}$$

the exact solution on an infinite domain is

$$U(x, t) = U_0 \exp[i\kappa(x - ct)], \tag{10}$$

where κ is the spatial wavenumber. Assuming a solution in the form

$$U(x,t) = u(t)\exp(i\kappa x) \tag{11}$$

and replacing the spatial derivative appearing in (8) by a numerical approximation, the following ordinary differential equation is obtained:

$$\frac{du}{dt} = -ic\kappa^* u = \lambda u, \tag{12}$$

where κ^* is the numerical (or modified) wavenumber, which depends on the spatial operator, and $\lambda = -ic\kappa^*$.

This ordinary differential equation can be numerically advanced in time using a time-march method. For linear time-march methods, the characteristic polynomial has one or more roots, σ, which are functions of λh, where h is the time step. We consider here only methods which produce one σ root. The numerical solution to (12) is then

$$u_n = U_0\sigma^n, \tag{13}$$

where $u_n = u(t_n) = u(nh)$. Writing $\sigma = R\exp(i\phi)$, the numerical solution to (8) is thus

$$U_{\text{num}}(x,t) = U_0 R^n \exp[i(\kappa x + n\phi)]. \tag{14}$$

This numerical solution can differ from the exact solution in both amplitude and phase. We can rewrite the numerical solution as

$$U_{\text{num}}(x,t) = U_0 R^n \exp[i\kappa(x - c^* t)], \tag{15}$$

where c^* is the numerical phase speed given by $c^* = \phi/\kappa h$. Comparing (15) with (10), we define the normalized error components as

$$er_a = |\sigma| - 1 = R - 1, \tag{16}$$

$$er_p = \frac{c^*}{c} - 1 = -\frac{\phi}{c\kappa h} - 1, \tag{17}$$

where er_a and er_p denote amplitude and phase error, respectively.

In one dimension, the error resulting from a given numerical scheme depends on the product $z = \kappa\Delta x$ where Δx is the grid spacing and the Courant number is $C = ch/\Delta x$. In two or three dimensions, the error has a further dependence on the direction of propagation. The two-dimensional linear convection equation is given by

$$\frac{\partial U}{\partial t} + c\cos\theta\frac{\partial U}{\partial x} + c\sin\theta\frac{\partial U}{\partial y} = 0. \tag{18}$$

This equation governs a plane wave convecting a scalar U with speed c along a straight line making an angle θ with respect to the x-axis. On a square grid, when the same difference operator is used to approximate the two spatial derivatives in (8), the two-dimensional numerical wavenumber κ^*_{2d} can be written as

$$\kappa^*_{2d}(z,\theta) = \cos\theta\kappa^*_{1d}(z\cos\theta) + \sin\theta\kappa^*_{1d}(z\sin\theta), \tag{19}$$

where κ^*_{1d} is determined from the one-dimensional analysis.

For the spatial operator given in (1), the numerical wavenumber is given by

$$i\kappa^* = \frac{1}{\Delta x}[d_0 + 2(d_1 \cos z + d_2 \cos 2z + d_3 \cos 3z) + 2i(a_1 \sin z + a_2 \sin 2z + a_3 \sin 3z)]. \tag{20}$$

For the time-marching method (4), σ is given by

$$\sigma = 1 + \lambda h + \beta_2(\lambda h)^2 + \beta_3(\lambda h)^3 + \beta_4(\lambda h)^4 + \beta_5(\lambda h)^5 + \beta_6(\lambda h)^6, \tag{21}$$

where

$$\beta_2 = \alpha_5, \quad \beta_3 = \alpha_5\alpha_4, \quad \beta_4 = \alpha_5\alpha_4\alpha_3,$$
$$\beta_5 = \alpha_5\alpha_4\alpha_3\alpha_2, \quad \beta_6 = \alpha_5\alpha_4\alpha_3\alpha_2\alpha_1.$$

The procedure for determining the errors for given values of z, θ, and C proceeds as follows. First, κ^*_{2d} must be calculated from (19) with κ^*_{1d} determined from (20). The parameter λ is then found using $\lambda = -ic\kappa^*$. Equation (21) is used to determine σ, which then produces the phase and amplitude errors from (16) and (17).

Figures 1 and 2 show the numerical phase speed and amplitude at a Courant number of unity in one dimension for the following three fully discrete finite-difference schemes: (1) second-order centered differences in space with fourth-order Runge–Kutta time marching (designated RK4C2 on the figures), (2) fourth-order centered differences with fourth-order Runge–Kutta time marching (designated RK4C4) and (3) the maximum-order spatial scheme given by (1) with $d_0 = 0.1$ and the time-marching method given by (4) with the values of the coefficients which produce the maximum order (designated maximum-order). Care must be taken in assessing schemes at individual values of θ and C. However, for the schemes considered here, the errors in the practical range of wavenumbers are generally largest for $\theta = 0^o$ and decrease with decreasing Courant number.

Lele [9] defines the resolving efficiency of a scheme as the fraction of the domain $0 \leq z \leq \pi$ for which the errors lie below a specified tolerance. Table 1 shows the resolving efficiency of the three schemes above for four different values of error tolerance e. In all three cases, the phase error is larger than the amplitude error and hence the resolving efficiency is determined by the phase error. Note that as the error tolerance decreases, the higher-order schemes become relatively more efficient. For example, at the largest error tolerance shown, the resolving efficiency of the maximum-order scheme is less than twice that of scheme RK4C4 while, at the smallest tolerance, the maximum-order scheme has almost three times the resolving efficiency of scheme RK4C4. The parameter $z = \kappa \Delta x$ is related to the number of points per wavelength by which a given wave is resolved through the relation $PPW = 2\pi/z$. Table 2 shows the *PPW* required to produce errors below the specified error tolerance values.

The procedure used to develop the optimized scheme is not sufficient to guarantee that the maximum error obtained over the specified wavenumber range in one dimension is not exceeded at nonzero values of θ. However, in the present case, the maximum phase and amplitude errors are obtained at $\theta = 0^o$ at a Courant number of unity. These errors are shown in Figures 3 and 4 in comparison with the maximum-order scheme for $0 \leq z \leq \pi/5$. The errors produced by the optimized scheme are bounded by 2×10^{-5} while the maximum-order scheme produces errors up to 4×10^{-4}. For the range $0.4 \leq z \leq 0.7$, the optimized scheme gives much smaller errors than the maximum-order scheme. This corresponds roughly to 9 to 16 *PPW*. For larger wavenumbers the advantage is reduced, while for smaller wavenumbers, the maximum-order scheme is more accurate.

Table 3 shows the resolving efficiency r and required *PPW* values for the optimized scheme with the four error tolerances as in the preceding tables. The advantage of the optimized

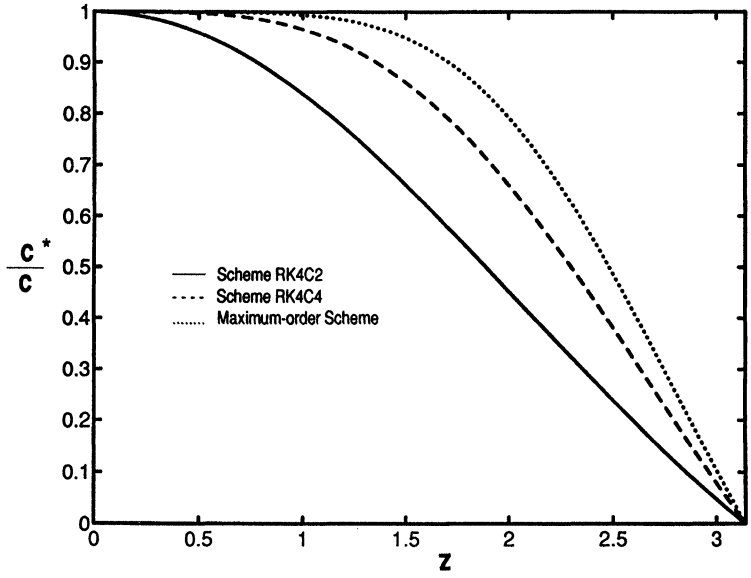

FIG. 1. *Numerical phase speed for second-order centered differences with fourth-order Runge–Kutta time marching* (RK4C2), *fourth-order centered differences with fourth-order Runge–Kutta time marching* (RK4C4), *and the maximum-order scheme.*

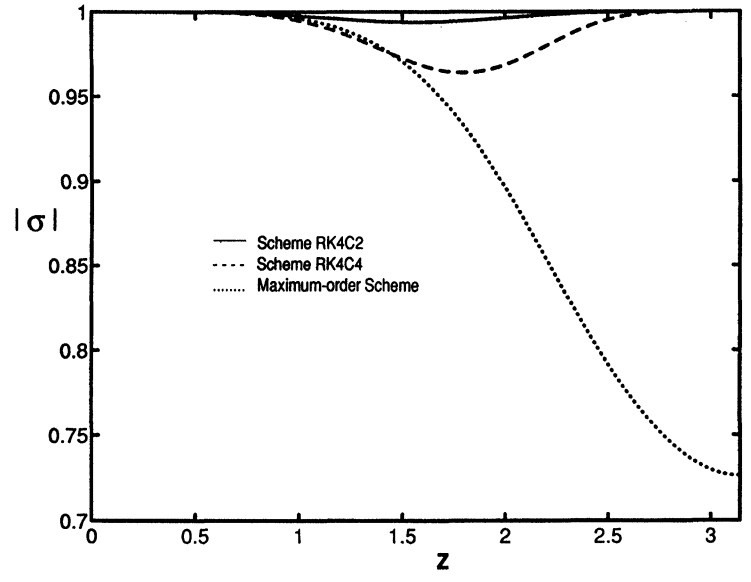

FIG. 2. $|\sigma|$ *for second-order centered differences with fourth-order Runge–Kutta time marching* (RK4C2), *fourth-order centered differences with fourth-order Runge–Kutta time marching* (RK4C4), *and the maximum-order scheme.*

scheme is largest at the "design" error tolerance 2×10^{-5}. For this error tolerance, it produces 1.6 times the resolving efficiency of the maximum-order scheme and four times the resolving efficiency of the fourth-order scheme. For error tolerances below 2×10^{-5}, the optimized

TABLE 1
Resolving efficiency of RK4C2, RK4C4, *and the maximum-order scheme.*

	e =			
Scheme	10^{-5}	2×10^{-5}	10^{-4}	3×10^{-3}
RK4C2	<0.01	<0.01	<0.01	0.04
RK4C4	0.04	0.05	0.07	0.17
Maximum order	0.11	0.12	0.16	0.29

TABLE 2
PPW required for specified error tolerances.

	e =			
Scheme	10^{-5}	2×10^{-5}	10^{-4}	3×10^{-3}
RK4C2	>200	>200	>200	50
RK4C4	50	40	29	12
Maximum order	18	17	13	7

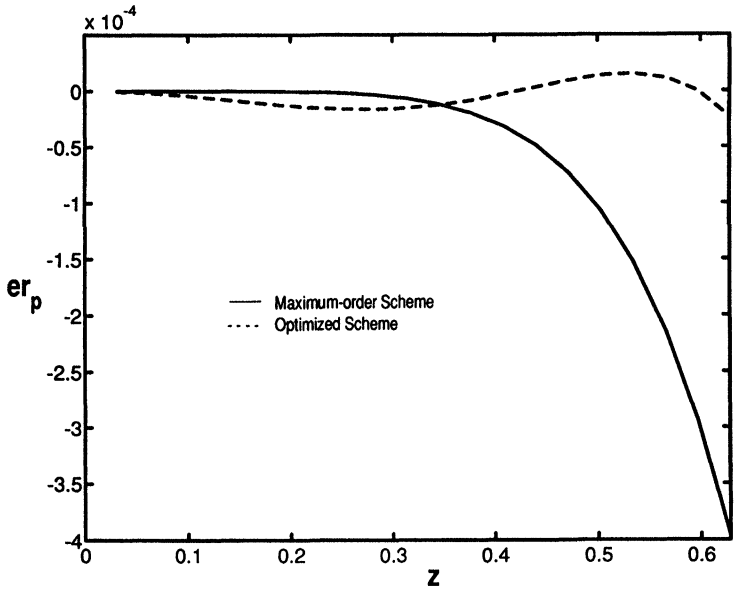

FIG. 3. *Phase error for the maximum-order scheme and the optimized scheme.*

scheme is substantially inferior to the maximum-order scheme. For higher values of error tolerance, the advantage of the optimized scheme is reduced in comparison with both the maximum-order scheme and the fourth-order scheme.

Another useful approach for assessing finite-difference schemes for wave propagation is to determine the *PPW* required to maintain global phase and amplitude errors below a specified level as a function of the number of wavelengths travelled. The global amplitude error is given by

$$Er_a = \left|1 - |\sigma(z, C)|^{\frac{2\pi n_w}{Cz}}\right|, \tag{22}$$

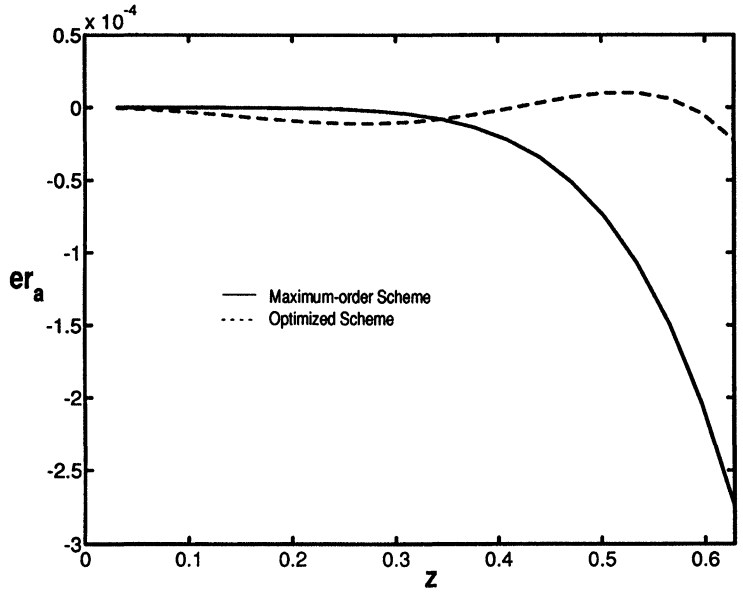

FIG. 4. *Amplitude error for the maximum-order scheme and the optimized scheme.*

TABLE 3
Resolving efficiency and PPW required for optimized scheme.

	e =			
	10^{-5}	2×10^{-5}	10^{-4}	3×10^{-3}
r	0.05	0.20	0.22	0.32
PPW	40	10	9	6

where n_w is the number of wavelengths travelled. The global phase error is

$$Er_p = \frac{2\pi n_w}{Cz}|\phi(C, z) + Cz|. \tag{23}$$

Figure 5 shows the *PPW* required to maintain Er_a and Er_p less than 0.1. The maximum-order scheme can accurately simulate the propagation of waves over distances greater than five hundred wavelengths with a grid resolution of less than twenty points per wavelength. This is less than half of the *PPW* required by the combination of fourth-order centered differences and fourth-order Runge-Kutta time marching. In three dimensions, this translates to more than eight times fewer grid nodes. The optimized scheme is superior for simulations in which waves travel under three hundred wavelengths. For such cases, good accuracy is obtained with roughly ten points per wavelength. In [21] several other finite-difference schemes are compared on this basis.

5. Stability and numerical boundary schemes. From Fourier analysis, the maximum-order fully discrete scheme is stable up to a Courant number of roughly 1.5 in one dimension and the optimized scheme is unconditionally unstable. Stability by Fourier analysis is a necessary condition for Lax-Richtmyer stability. However, the instability of the optimized scheme is very mild and we now show that on a finite domain asymptotic (or time) stability is achieved. Consider a semidiscrete approximation to (8) obtained by dividing the domain into

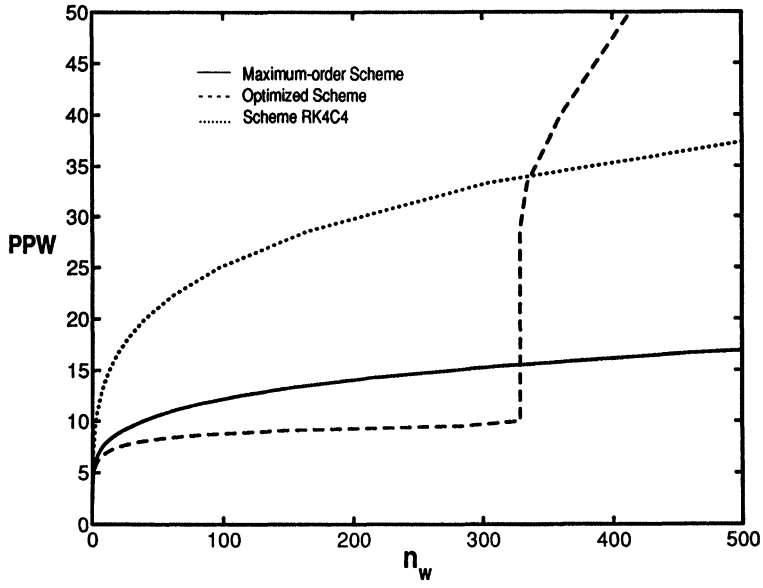

FIG. 5. *PPW requirements for the maximum-order scheme, the optimized scheme, and the combination of fourth-order centered differences and fourth-order Runge–Kutta time marching.*

M subintervals of length $\Delta x = 1/M$ and approximating the spatial derivative in the interior by (1). At the inflow boundary, the derivative is approximated by [18]:

$$(\delta_x u)_1 = \frac{1}{60\Delta x}[-12u_0 - 65u_1 + 120u_2 - 60u_3 + 20u_4 - 3u_5],$$
$$(\delta_x u)_2 = \frac{1}{60\Delta x}[6.6u_0 - 51.6u_1 + 34u_2 - 12u_3 + 39u_4 - 19.6u_5 + 3.6u_6]. \tag{24}$$

These operators are fifth-order accurate and hence do not compromise the global accuracy of the method. At the outflow boundary, the difference operators for the last three points in the grid are formed using fifth-order space extrapolation together with the interior differencing scheme. The space extrapolation can be written in the form

$$(1 - E^{-1})^p u_{M+1} = 0, \tag{25}$$

where the shift operator E is defined by $Eu_j = u_{j+1}$ and the order of the approximation is $p - 1$. When this approach is applied to hyperbolic systems, flux-vector splitting is required near boundaries [20].

The semidiscrete form can be written as

$$\frac{d\mathbf{u}}{dt} = \tilde{\mathbf{A}}\mathbf{u}, \qquad \text{where} \qquad \tilde{\mathbf{A}} = \frac{c}{\Delta x}\mathbf{A}, \tag{26}$$

$\mathbf{u} = [u_1, u_2, \ldots, u_{M-1}, u_M]^T$. Figure 6 shows the eigenvalues of $\mathbf{A}$ for the maximum-order and optimized spatial schemes with $M = 100$. Each scheme produces two boundary-condition-dependent eigenvalues [2] but these lie in the left half-plane and hence do not pose a problem. These eigenvalue spectra both lie well within the stability contours of the respective time-marching methods, as shown in Figure 7, and thus the fully discrete methods are asymptotically stable at a Courant number of unity.

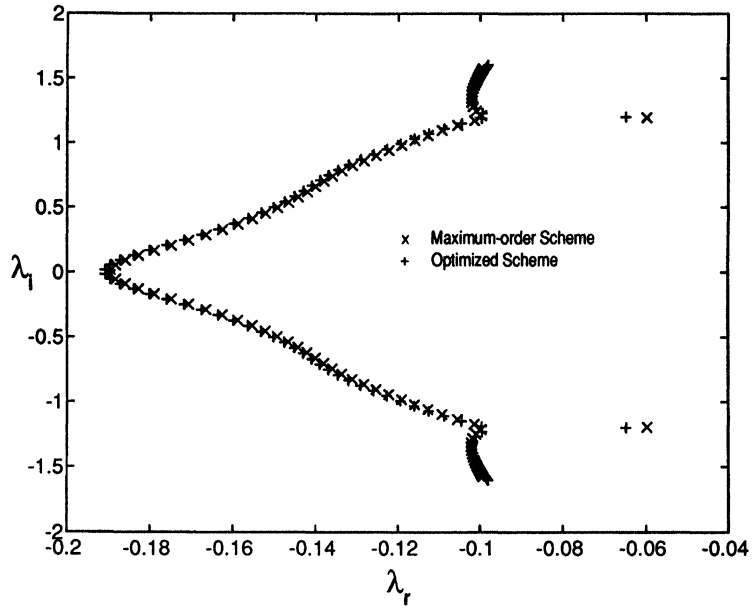

FIG. 6. *Eigenvalue spectra of semidiscrete operators.*

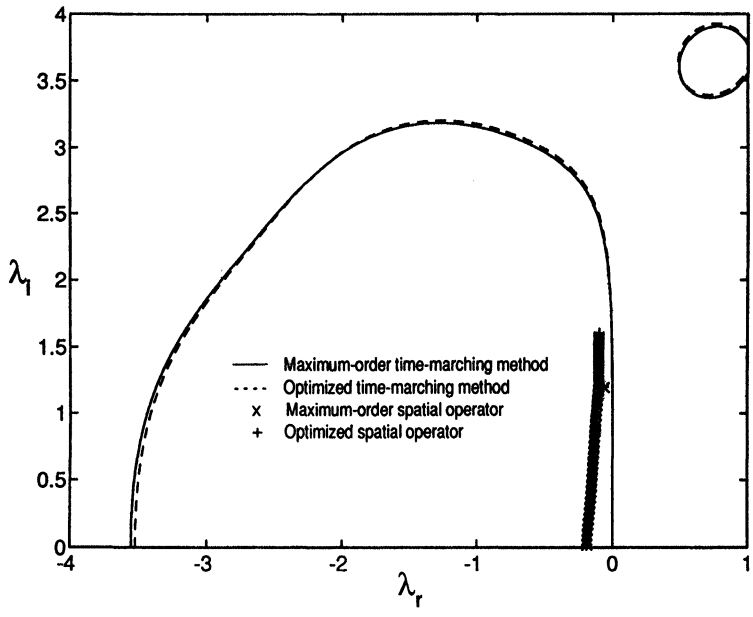

FIG. 7. *Stability contours of the time-marching methods.*

Asymptotic stability is a necessary condition for Lax-Richtmyer stability but it is not sufficient. Thus we now consider the amplification matrix **G** given by

$$\mathbf{G} = \mathbf{I} + C\mathbf{A} + \beta_2(C\mathbf{A})^2 + \beta_3(C\mathbf{A})^3 + \beta_4(C\mathbf{A})^4 + \beta_5(C\mathbf{A})^5 + \beta_6(C\mathbf{A})^6. \tag{27}$$

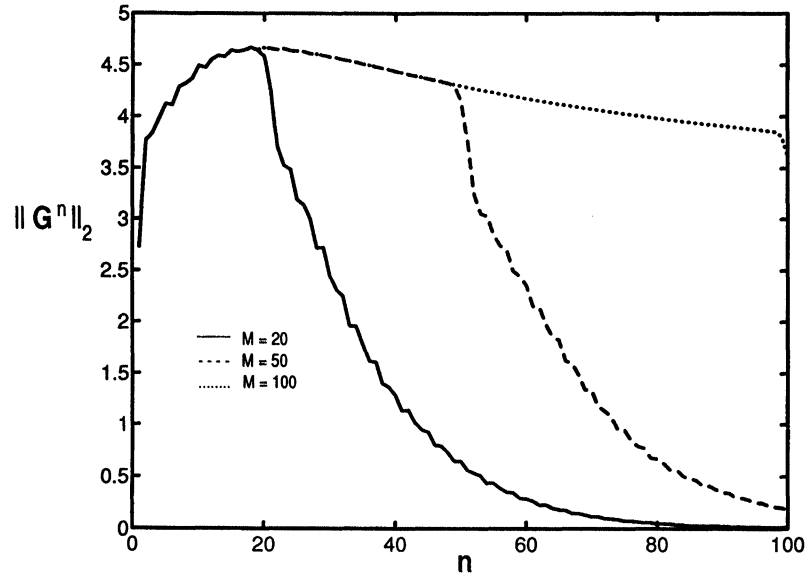

FIG. 8. *Variation of the L_2-norm of the amplification matrix of the maximum-order scheme.*

A necessary and sufficient condition for stability of a fully discrete finite-difference scheme is that there exists a constant $K \geq 1$ such that

$$\|(\mathbf{G}(\Delta x, h))^n\| \leq K \tag{28}$$

for all $n \geq 0$, $0 \leq nh \leq T$ with T fixed. For hyperbolic problems, the Courant number must be kept constant as n is increased. Figure 8 shows $\|\mathbf{G}^n\|_2$ for the maximum-order scheme for three different values of M and a Courant number of unity. Figure 9 shows similar results for the optimized scheme. In both cases, $\|\mathbf{G}^n\|_2$ is clearly bounded and hence both schemes appear to be stable. This is consistent with the results of [20], in which both schemes were used for simulations of electromagnetic waves with no evidence of instability. However, a singular value decomposition of $\mathbf{G}^n$ shows that the growth in $\|\mathbf{G}^n\|$ shown in Figure 9 is associated with the numerical boundary scheme at the inflow boundary. This obscures the very slow growth of the unstable modes of the optimized scheme, which is revealed if the numerical boundary scheme at inflow is removed. Nevertheless, Figure 9 provides some reassurance that the instability causes no immediate difficulties. As shown in Figure 4, the maximum value of $|\sigma|$ predicted using Fourier analysis is 1.00002 at a Courant number of unity. Since $1.00002^{34,000} < 2$, the scheme can safely be used for well over 34,000 time steps without the solution exhibiting any instability. However, the optimized scheme is not intended for such long simulations since the maximum-order scheme becomes more accurate if the distance travelled becomes very large, as shown in Figure 5.

6. Numerical experiments. We now consider several numerical experiments in order to further compare the four schemes discussed above. The one-dimensional linear convection equation with $c = 1$ is solved with periodic boundary conditions on the domain $0 \leq x \leq 1$. The initial condition is given by a Gaussian-modulated cosine function as follows:

$$U(x, 0) = (\cos \kappa x) e^{-0.5[(x-0.5)/\sigma_g]^2}$$

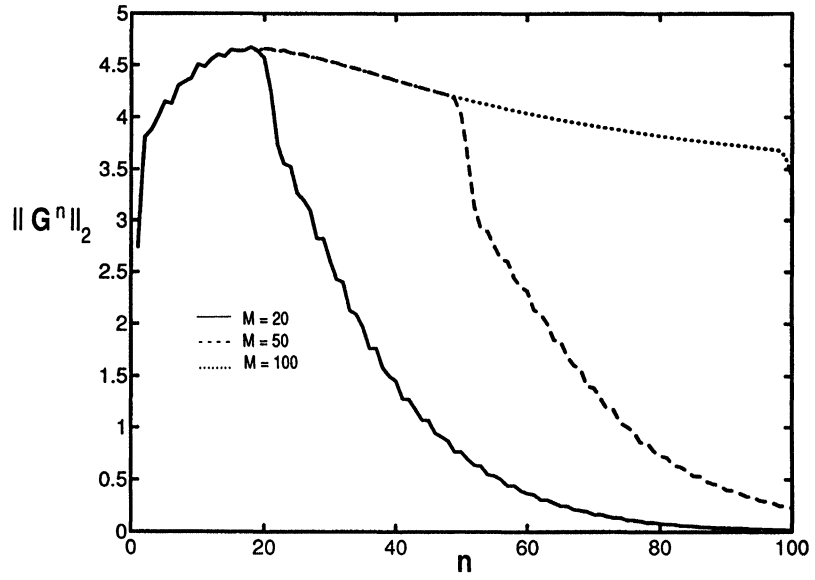

FIG. 9. *Variation of the L_2-norm of the amplification matrix of the optimized scheme.*

with various values of σ_g and κ. For the present schemes, the errors in the practical range of wavenumbers are generally largest at $\theta = 0^o$ and decrease with decreasing Courant number. Therefore, one-dimensional numerical experiments with a Courant number of unity represent the worst case.

For the first experiment, we consider a Gaussian ($\kappa = 0$) with $\sigma_g = 0.04$. The grid is uniform with 100 points across the domain. Figure 10 shows the result after 100 time steps with a Courant number of unity, i.e., at $t = 1$. The exact solution is identical to the initial condition. The solution produced by scheme RK4C2 is poor, while the other schemes are very accurate. After 1000 time steps, the solution produced by RK4C4 is inadequate for many purposes, while the maximum-order and optimized schemes remain very accurate, as shown in Figure 11.

Figures 12–15 compare the maximum-order and optimized schemes for Gaussian initial conditions with four different values of σ_g. The results are again shown for $C = 1$ and $t = 1$. The figures show the difference between the computed solution and the exact solution. For $\sigma_g = 0.04$ and $\sigma_g = 0.03$, the L_2-norm of the error produced by the optimized scheme is less than half of that produced by the maximum-order scheme. For $\sigma_g = 0.02$ the improvement from the optimized scheme is reduced and for $\sigma_g = 0.05$ the optimized scheme produces more error than the maximum-order scheme.

These results can be better understood by considering the normalized power spectra of these Gaussians, which are shown in Figure 16. These spectra show the wavenumber content of the Gaussians as a function of z based on a 100-point grid. They can be compared with Figures 3 and 4, which show the numerical errors also as a function of z. For example, Figures 3 and 4 show that the optimized scheme is much more accurate than the maximum-order scheme for roughly $0.4 \leq z \leq 0.7$. With $\sigma_g = 0.05$, there is virtually no content in this region and hence the optimized scheme is inferior to the maximum-order scheme since it produces more error at low wavenumbers. For $\sigma_g = 0.04$ and $\sigma_g = 0.03$, there is some content in the range $0.4 \leq z \leq 0.7$ and little content at higher wavenumbers. Consequently, the error is dominated by these modes and the optimized scheme is superior. Finally, for $\sigma_g = 0.02$, the

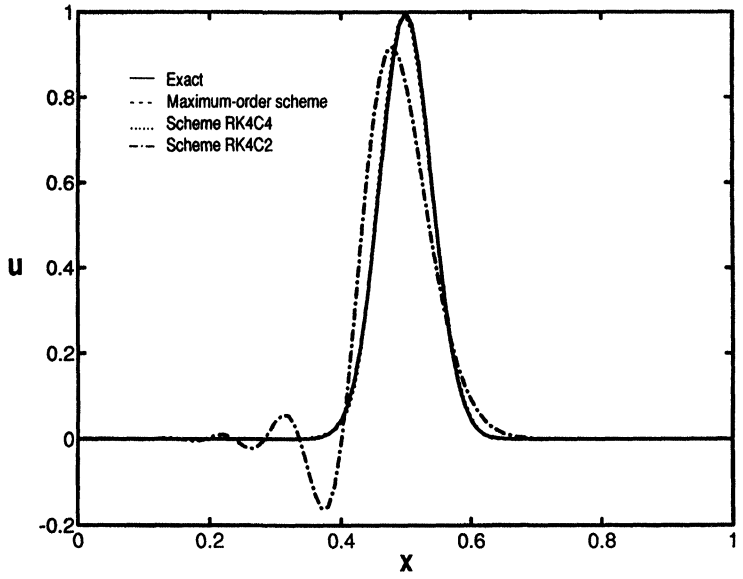

FIG. 10. *Solution at* $t = 1$.

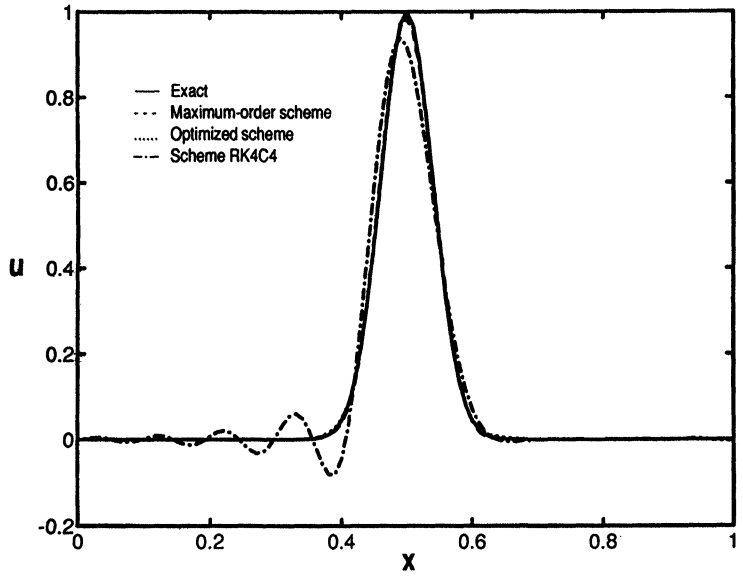

FIG. 11. *Solution at* $t = 10$.

error is dominated by wavenumbers with $z > 0.7$ and thus the optimized scheme is not much superior to the maximum-order scheme.

The gains produced by the optimized scheme for Gaussians are quite modest, even for $\sigma_g = 0.03$ and $\sigma_g = 0.04$. This occurs because Gaussians always have considerable low wavenumber content, which is convected more accurately by the maximum-order scheme. The optimized scheme is more effective for functions with a narrower bandwidth. Figures 17-19 show results for Gaussian-modulated cosine functions with $\sigma_g = 0.1$ and $\kappa = 24\pi$,

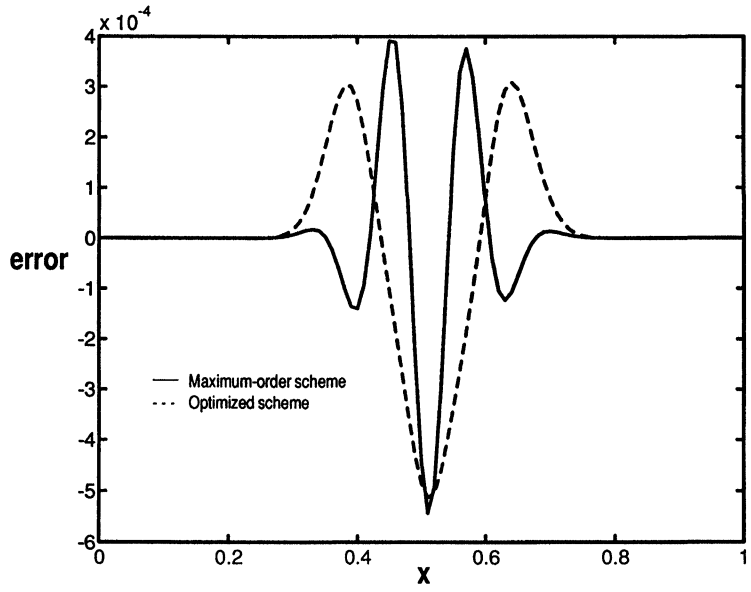

FIG. 12. *Error for* $\sigma_g = 0.05$.

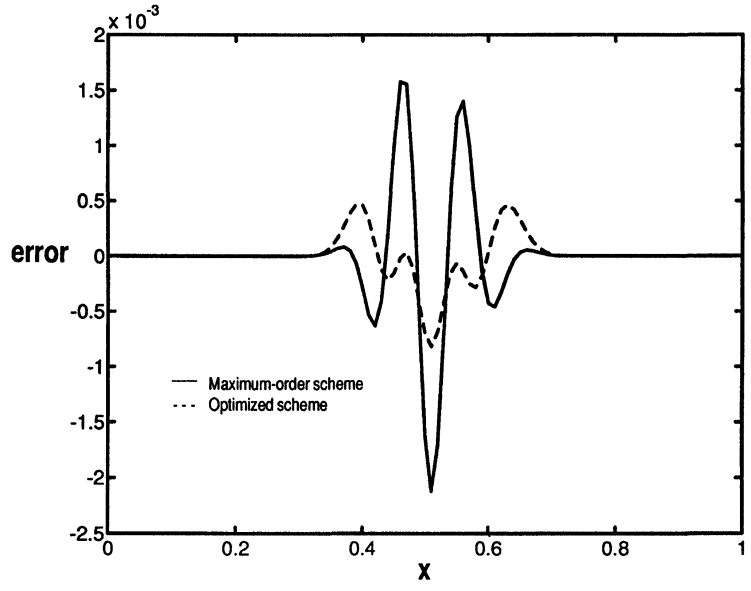

FIG. 13. *Error for* $\sigma_g = 0.04$.

32π, and 40π, on a 200-point grid. The results are shown after 200 time steps at a Courant number of unity, i.e., at $t = 1$. The corresponding normalized power spectra are shown in Figure 20. In each case, these functions have considerable spectral content in the range for which the optimized scheme is superior. For $\kappa = 32\pi$, the L_2-norm of the error produced by the optimized scheme is more than ten times less than that produced by the maximum-order scheme.

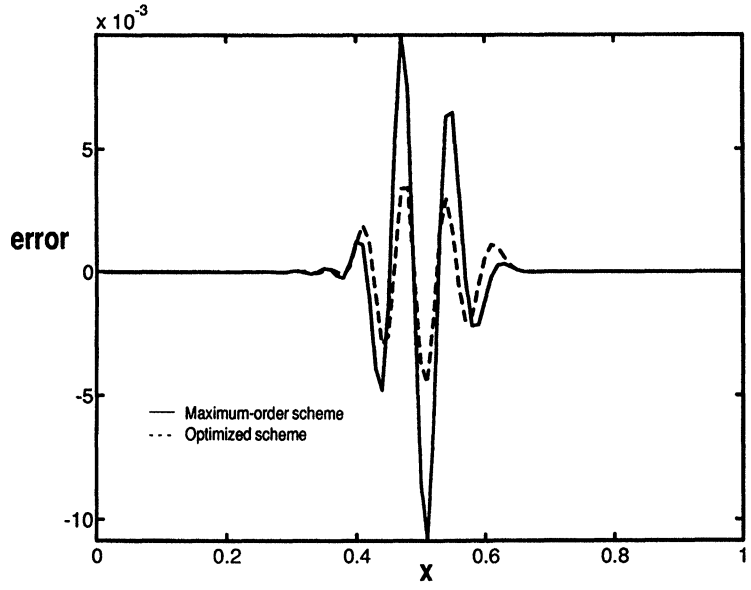

FIG. 14. *Error for* $\sigma_g = 0.03$.

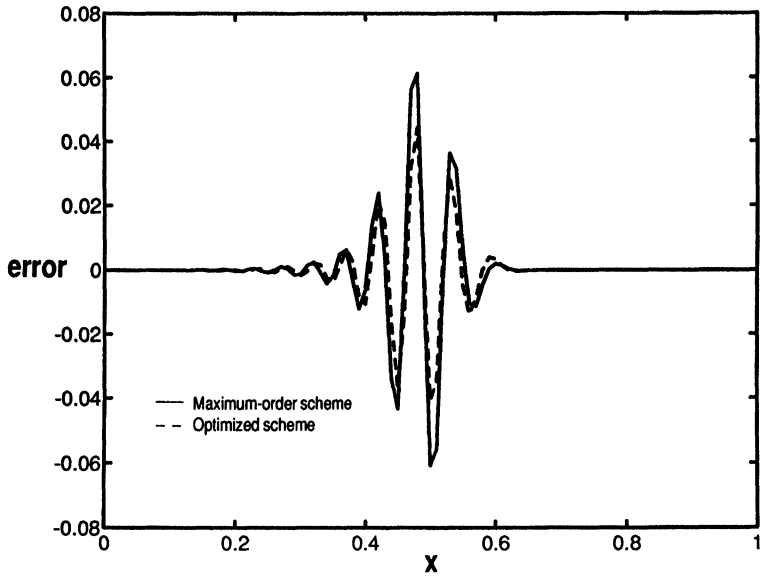

FIG. 15. *Error for* $\sigma_g = 0.02$.

7. Discussion. In this section, we discuss some considerations in selecting and developing finite-difference schemes for wave propagation problems. Initially an error tolerance must be determined. This is based on two factors: (1) the level of accuracy required of the simulation in order to produce meaningful results and (2) an estimate of the largest distance a wave will travel during the simulation. Next an estimate must be made of the shortest wavelength which must be accurately resolved. This is also based on the accuracy requirements of the sim-

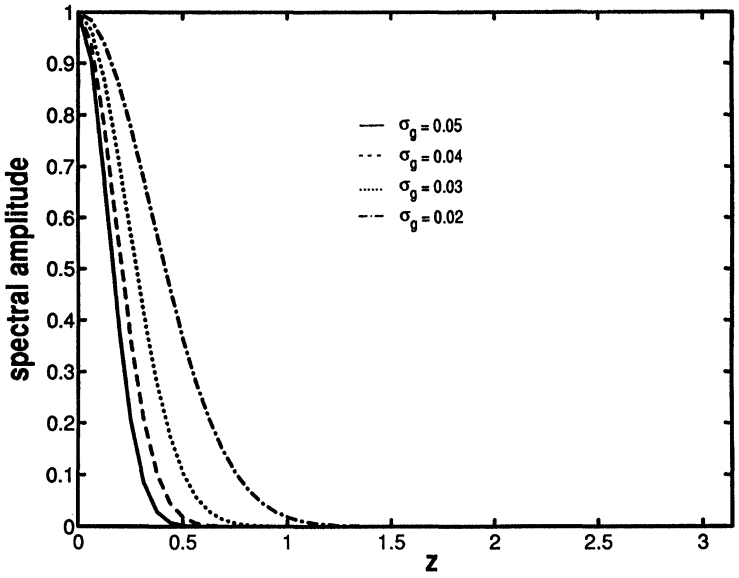

FIG. 16. *Normalized power spectra of Gaussians.*

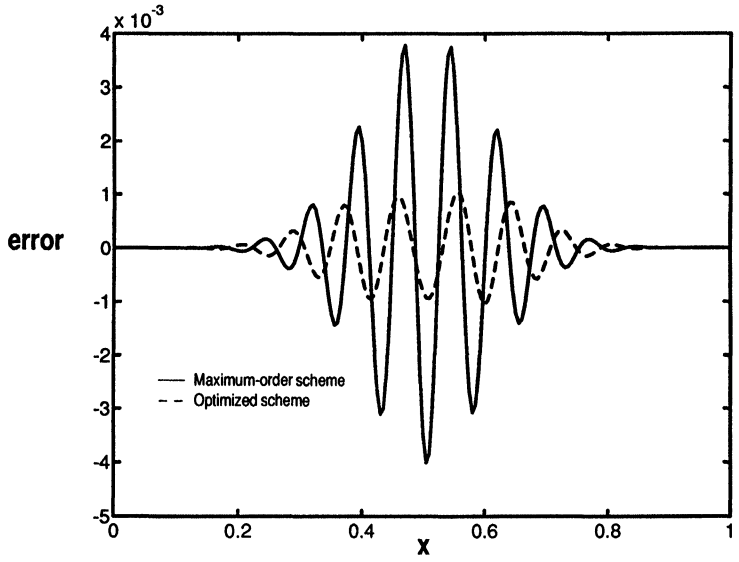

FIG. 17. *Error for* $\kappa = 24\pi$.

ulation. For a given scheme, the grid spacing can then be determined to produce the required accuracy in phase and amplitude for the shortest wavelength of interest based on Fourier error analysis. The grid resolution must be sufficient to satisfy the accuracy requirements for the worst combination of Courant number and propagation direction.

The compromise involved in optimizing a scheme is clearly revealed in Figure 5. For small distances of travel, the optimized scheme is superior but as the distance is increased the maximum-order scheme eventually requires fewer *PPW*. [21] includes a scheme similar to

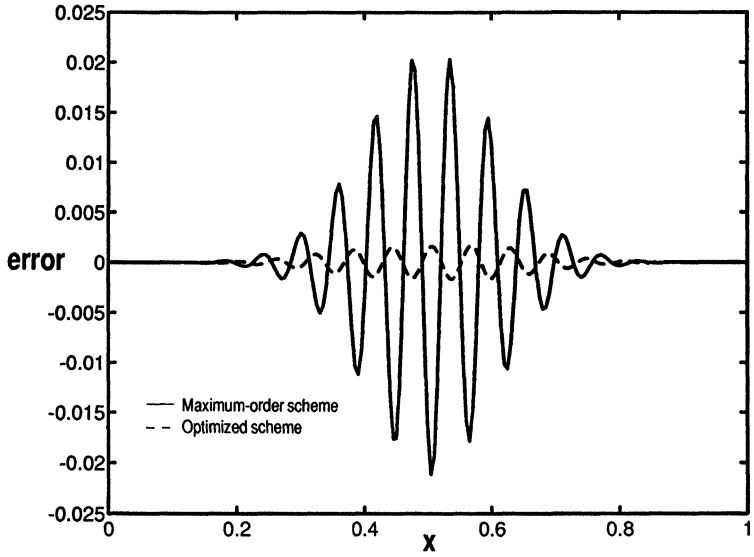

FIG. 18. *Error for* $\kappa = 32\pi$.

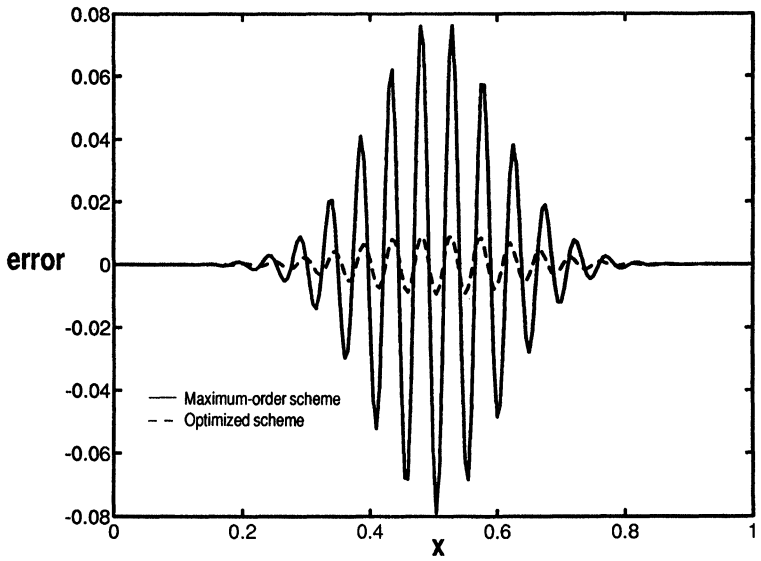

FIG. 19. *Error for* $\kappa = 40\pi$.

that presented here which is optimized for waves resolved with at least 7.5 *PPW*. This scheme is slightly superior to the present optimized scheme for distances of travel less than roughly 75 wavelengths but is inferior for longer distances.

For some wave propagation applications, it is essential that the numerical scheme produce no dissipation, i.e., no amplitude error. The schemes presented here are inappropriate for such problems. However, for most problems it is sufficient that the amplitude error be less than or comparable to the phase error. Furthermore, the damping of high wavenumber modes produced by the present schemes can be helpful in some applications [17]. If reduced dissipation is

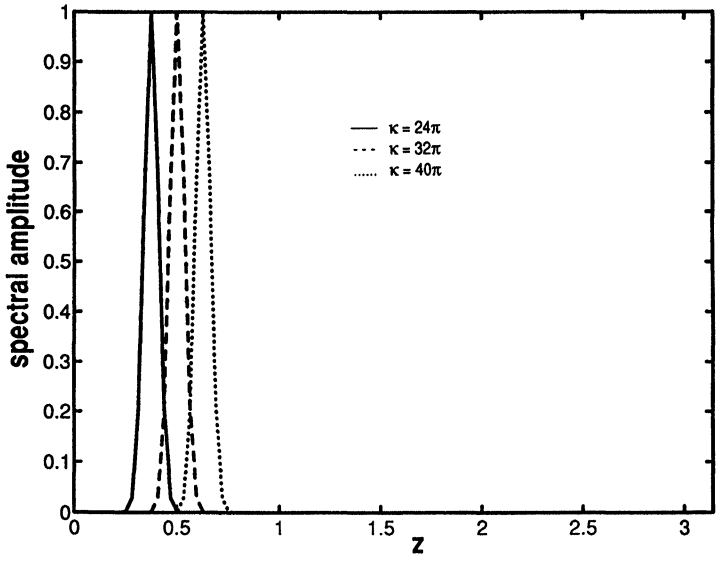

FIG. 20. *Normalized power spectra of Gaussian-modulated cosine functions.*

desired, the present spatial scheme can be used without the filter. Fourth-order Runge-Kutta time marching should then be used for stability.

8. Conclusions. The two finite-difference schemes presented here provide a promising option for simulating long-range propagation of linear waves. Potential applications include electromagnetics and acoustics. Both schemes combine a seven-point spatial operator and an explicit six-stage low-storage time-marching method of the Runge-Kutta type. The optimized scheme was developed by minimizing the maximum phase and amplitude errors for waves which are resolved with at least ten points per wavelength. The maximum-order scheme can accurately simulate the propagation of waves over distances greater than five hundred wavelengths with a grid resolution of less than twenty points per wavelength. The optimized scheme is intended for simulations in which waves travel under three hundred wavelengths. For such cases, good accuracy is obtained with roughly ten points per wavelength. Future work will address the application of these schemes to complex geometries.

REFERENCES

[1] R. M. ALFORD, K. R. KELLY, AND D. M. BOORE, *Accuracy of finite-difference modeling of the acoustic wave equation*, Geophysics, 39 (1974), pp. 834-842.

[2] R. M. BEAM AND R. F. WARMING, *The asymptotic spectra of banded Toeplitz and quasi-Toeplitz matrices*, SIAM J. Sci. Comput., 14 (1993), pp. 971-1006.

[3] C. L. CHEN, S. R. CHAKRAVARTHY, AND B. L. BIHARI, *Numerical Solution of Acoustic Equations with Unstructured Grids Using a CFD-Based Approach*, AIAA Paper 92-2698, American Institute of Aeronautics and Astronautics, New York, 1992.

[4] G. COHEN AND P. JOLY, *Fourth order schemes for the heterogeneous acoustics equation*, Comput. Methods Appl. Mech. Engrg., 80 (1990), pp. 397-407.

[5] M. A. DABLAIN, *The application of high-order differencing to the scalar wave equation*, Geophysics, 51 (1986), pp. 54-66.

[6] S. DAVIS, *Matrix-Based Finite Difference Algorithms for Computational Acoustics*, AIAA Paper 90-3942, American Institute of Aeronautics and Astronautics, New York, 1990.

[7] ———, *Low-dispersion finite difference methods for acoustic waves in a pipe*, J. Acoust. Soc. Amer., 90 (1991), pp. 2775-2781.

[8] O. HOLBERG, *Computational aspects of the choice of operator and sampling interval for numerical differentiation in large-scale simulation of wave phenomena*, Geophys. Prospecting, 35 (1987), pp. 629-655.

[9] S. K. LELE, *Compact finite difference schemes with spectral-like resolution*, J. Comput. Phys., 103 (1992), pp. 16-42.

[10] K. J. MARFURT, *Accuracy of finite-difference and finite-element modeling of the scalar and elastic wave equations*, Geophysics, 49 (1984), pp. 533-549.

[11] P. SGUAZZERO, M. KINDELAN, AND A. KAMEL, *Dispersion-bounded numerical integration of the elastodynamic equations with cost-effective staggered schemes*, Comput. Methods Appl. Mech. Engrg., 80 (1990), pp. 165-172.

[12] V. SHANKAR, A. H. MOHAMMADIAN, AND W. F. HALL, *A time-domain finite-volume treatment for the Maxwell's equations*, Electromagnetics, 10 (1990), pp. 127-147.

[13] A. TAFLOVE, *Re-inventing Electromagnetics: Supercomputing Solution of Maxwell's Equations Via Direct Time Integration on Space Grids*, AIAA Paper 92-0333, American Institute of Aeronautics and Astronautics, New York, 1992.

[14] C. K. W. TAM, *Discretization Errors Inherent in Finite Difference Solution of Propellor Noise Problems*, AIAA J., 30 (1992), pp. 608-615.

[15] C. K. W. TAM AND J. C. WEBB, *Dispersion-relation-preserving finite difference schemes for computational acoustics*, J. Comput. Phys., 107 (1993), pp. 262-281.

[16] R. VICHNEVETSKY AND J. B. BOWLES, *Fourier Analysis of Numerical Approximations of Hyperbolic Equations*, Society for Industrial and Applied Mathematics, Philadelphia, PA, 1982.

[17] M. YARROW, J. A. VASTANO, AND H. LOMAX, *Pulsed Plane Wave Analytic Solutions for Generic Shapes and the Validation of Maxwell's Equations Solvers*, AIAA Paper 92-0016, American Institute of Aeronautics and Astronautics, New York, 1992.

[18] D. W. ZINGG AND H. LOMAX, *On the eigensystems associated with numerical boundary schemes for hyperbolic equations*, in Numerical Methods for Fluid Dynamics, M. J. Baines and K. W. Morton, eds., Clarendon Press, Oxford, 1993, pp. 473-481.

[19] ———, *Some Aspects of High-Order Numerical Solutions of the Linear Convection Equation with Forced Boundary Conditions*, AIAA Paper 93-3381 in the Proc. of the 11th AIAA Computational Fluid Dynamics Conf., American Institute of Aeronautics and Astronautics, New York, 1993.

[20] D. W. ZINGG, P. D. GIANSANTE, AND H. M. JURGENS, *Experiments with High-Accuracy Finite-Difference Schemes for the Time-Domain Maxwell Equations*, AIAA Paper 94-0232, American Institute of Aeronautics and Astronautics, New York, 1994.

[21] D. W. ZINGG, E. M. EPSTEIN, AND H. M. JURGENS, *A Comparison of Finite-Difference Schemes for Computational Aeroacoustics*, AIAA Paper 95-0162, American Institute of Aeronautics and Astronautics, New York, 1995.